The CSI Journal on
Computer Science and Engineering
Vol. 18, No. 1, 2020
Pages 44-53
Regular Research Paper

Guided Ridge Regression-Based Polarimetric-Spatial Feature Extraction for Classification of Polarimetric SAR Images

Maryam Imani

Faculty of Electrical and Computer Engineering, Tarbiat Modares University

Abstract

Synthetic aperture radar (SAR) acquires high resolution images containing rich spatial information. The Polarimetric SAR (PolSAR) images are a good source of polarimetric and spatial information appropriate for land cover classification. Two PolSAR image classification methods are introduced in this work: ridge regression-based polarimetric-spatial (RRPS) and the guided RRPS. The RRPS feature extraction method generates polarimetric-spatial features with minimum overlapping and redundant information. To this end, each polarimetric-spatial channel of the PolSAR data is represented through a ridge regression model using the farthest neighbors of that channel. The weights of the regression model compose the projection matrix for dimensionality reduction. The guided RRPS method uses the weights of the guided filter to revise the probability maps corresponding to the initial classification map. The proposed RRPS and guided RRPS methods show high performance for PolSAR image classification in small sample size situations.

Keywords: Ridge regression, Polarimetric SAR, feature space projection, classification, guided filter.

1. Introduction

The development of radar remote sensors in recent years allows high resolution imagery in any time and weather conditions [1]. Polarimetric synthetic aperture radar (PolSAR) allows ground surface classification with high precision by providing SAR images in multiple polarimetric channels [2]. However, the PolSAR image classification is a challenging task. Materials from different classes may have similar polarimetric signatures or samples belonging to the same class may have dissimilar polarimetric signatures which lead to mis-classification. On the other hand, proper extraction of spatial features from high resolution PolSAR images is important. SAR images are often contaminated by speckle noise, which hardens spatial feature extraction with keeping details and preserving the class boundaries [3].

Generally, the researches in the PolSAR classification application are divided into three categories. The first category focuses on processing of polarimetric information through various target decomposition methods [4]-[5]. The Intrinsic features obtained by Laplacian eigenmaps, called LE-IF, provide a polarimetric feature space with reduced dimensionality [6]. LE-IF is a nonlinear and manifold-based dimensionality reduction method, which provides a compact feature space from a high dimensional polarimetric feature space. The second category of PolSAR classification methods focuses on contextual feature extraction [7]-[8] and the third one tries to integrate polarimetric and contextual characteristics [9]-[10]. The feature attribute profiles (FPs) method has been introduced for extraction of contextual features from the SAR image [11]. The high-level attribute features extracted by FPs provide superior classification results. FPs can be extended to PolSAR images by applying FPs on each principal component of the PolSAR cube. Applying FPs on PolSAR can result in an appropriate polarimetric-spatial feature cube.

Several works have studied polarimetric and contextual feature fusion to improve the PolSAR image classification. A hybrid conditional random fields model based on complex-valued three-dimensional convolutional neural networks is introduced in [12]. It combines the representation learning ability of deep learning with the modeling power of random fields for PolSAR image classification. This method enhances the classification accuracy in edge locations and is robust against speckle noise. In [13], an online multiview deep forest architecture is suggested, which consists of multiple layers. Each layer is an ensemble of multiple random forests where they are process data from different views. The method learns a deep forest model from a stream of multiview data in an online manner. The experiments show high accuracy of this model, especially on small-scale training data.

An object-oriented land cover PolSAR classification method is proposed in [14], which integrates the dual-channel Watershed region merging segmentation and a Bagging-based ensemble extreme learning. The object-based classifiers can be useful to reduce the speckle noise. In [15], a texture classification-based nonlocal means PolSAR filter is introduced. In the suggested process, a classification algorithm, which identifies the data into textural variations and heterogeneity, is presented. In addition, a similarity metric is obtained for estimation of the patch similarity of *K*-distributed covariance matrices. The filtering-based method is capable to reduce the speckle along with edges and preserving the details.

The proposed methods in this work belong to the third category. The proposed methods use the ability of morphological filters [16]-[17] for contextual feature extraction to provide a polarimetric-contextual cube. The aim of the proposed methods is to find a reduced subset of polarimetric-morphological features with minimum redundant information. To this end, each feature of the polarimetric-contextual cube is represented by a linear combination of its farthest neighbors to achieve features with the lowest overlapping. The normalized weights of the ridge regression model are used to compose the projection matrix. The first proposed method called ridge regression-based polarimetric-spatial (RRPS) feature extraction uses the mean vectors of all classes in each channel as a representative of that channel. Due to using the first-order statistics, RRPS has high efficiency using limited training samples. In addition, its objective function has a simple and closed form solution.

To degrade the negative effect of speckle noise and to align the classification maps with the real class boundaries, the obtained probability maps associated with the achieved classification map are optimized by applying the guided filters [18]-[20]. Eventually, the final classification map is obtained by choosing the maximum probabilities of C classes. This revised RRPS is called guided RRPS. The performances of the proposed RRPS and guided RRPS are compared with several methods in terms of several measures and on four PolSAR datasets. The experimental results show superior performance of guided RRPS and RRPS by only using 5 training samples per class.

This paper is organized as follows. The proposed RRPS and guided RRPS methods are introduced with more details in section 2. The experimental results are discussed in section 3, and finally, section 4 concludes the paper.

2. Proposed Guided RRPS

Associated with each pixel of the PolSAR image, there is a coherency matrix as follows:

$$\boldsymbol{T} = \begin{bmatrix} T_{11} & T_{12} & T_{13} \\ T_{12}^* & T_{22} & T_{23} \\ T_{13}^* & T_{23}^* & T_{33} \end{bmatrix} \quad (1)$$

where $(\cdot)^*$ indicates the conjugate operator. Each pixel of the PolSAR image can be represented by a 9×1 feature vector:

$$\boldsymbol{f} = [T_{11}, T_{22}, T_{33}, Re(T_{12}), Im(T_{12}), Re(T_{13}), Im(T_{13}), Re(T_{23}), Im(T_{23})] \quad (2)$$

where $Re(\cdot)/Im(\cdot)$ denotes the real/imaginary part of $(\cdot)$ and $T_{ij}; i, j = 1,2,3$ are the elements of matrix $\boldsymbol{T}$ in (1). So, the PolSAR cube is considered as a $a \times b \times 9$ cube in this work where r/c is the number of rows/columns of the PolSAR image. This cube is represented by Pol.

The ridge regression-based polarimetric-spatial (RRPS) and guided RRPS feature extraction methods are proposed for PolSAR image classification in this work. RRPS is inspired from our previous work, feature extraction based on ridge regression for hyperspectral image classification [21]. In PolSAR images, the use of only polarimetric channels is not sufficient for having an accurate classification map. The reason is that some pixels from different classes may have similar polarimetric signatures or samples from the same class may have different polarimetric features. So, the use of contextual information can be very helpful for classification. In addition, due to high resolution of SAR images, the use of spatial information is absolutely reasonable.

Morphological profiles (MPs) achieved by morphological filters by reconstruction have shown great success for contextual feature extraction in various optical and radar images. In addition, they have simple implementation. So, in this work, MP of the PolSAR data is obtained firstly. To this end, the principal component analysis (PCA) transform [22] is applied to the PolSAR cube and the first three components (PCs) are extracted. An MP is constructed on each PC. Then, MPs are concatenated. The result is MP of the PolSAR cube. The original PolSAR cube (Pol) is stacked on its MP to integrate the polarimetric and morphological channels denoted as Pol+MP, a polarimetric-spatial cube with b channels. The dimensionality of Pol+MP is high particularly when limited training samples are available. In addition, there is redundant information among different channels, which should be removed. To this end, feature reduction is a necessity.

2.1. RRPS

The proposed RRPS method uses the first-order statistics of data (mean vectors) to have good performance using a small training set. Let m_{ij} $(i = 1, 2, \dots, b; j = 1, 2, \dots, C)$ denotes the mean of training samples of class j in ith channel of the PolSAR cube. In each channel, the mean vector of each channel of Pol+MP, denoted as $\boldsymbol{h}_i$; $i = 1, 2, \dots, b$, is defined by:

$$\boldsymbol{h}_i = [m_{i1} \quad m_{i2} \quad \cdots \quad m_{iC}]^T \tag{3}$$

where it contains the mean value of C classes in channel i. The aim is to extract m polarimetric-spatial features from b channels of the original Pol+MP cube by applying a projection matrix as $\boldsymbol{y}_{m\times 1} = \mathbf{A}_{m\times b}\boldsymbol{x}_{b\times 1}$ $(m < b)$. The extracted features should be such a way that they have the least overlapping in the polarimetric-spatial feature space. In other words, they should be as far as possible with respect to each other in the polarimetric-spatial feature space. To this end, consider $\boldsymbol{h}_i$ as a central polarimetric-spatial feature vector dented by $\boldsymbol{q}_i = \boldsymbol{h}_i$. Then, find m farthest neighbors of $\boldsymbol{q}_i$ among $\boldsymbol{h}_j (j = 1,2,..,b\,; j \neq i)$, in other words the vectors with the largest Euclidean distance $\|\boldsymbol{q}_i - \boldsymbol{h}_j\|^2; j = 1,2,..,b\,; j \neq i$. The m farthest neighbors are denoted by $\boldsymbol{h}_{i1}, \boldsymbol{h}_{i2}, \dots, \boldsymbol{h}_{im}$. Then, the central vector $\boldsymbol{q}_i$ is represented by using a linear regression as follows:

$$\boldsymbol{q}_i = w_{i1}\boldsymbol{h}_{i1} + w_{i2}\boldsymbol{h}_{i2} + \cdots + w_{im}\boldsymbol{h}_{im} + \boldsymbol{\varepsilon} \;; \quad i = 1,2,\dots,b \tag{4}$$

where $\boldsymbol{\varepsilon}$ is the disturbance term and $w_{i1}, w_{i2}, \dots, w_{im}$ are weights of the regression. With definition of

$$\mathbf{H}_i = [\boldsymbol{h}_{i1}\ \boldsymbol{h}_{i2} \dots \boldsymbol{h}_{im}] \;; i = 1,2,\dots,b \tag{5}$$

$$\boldsymbol{w}_i = [w_{i1}\ w_{i2} \dots w_{im}]^T \;; i = 1,2,\dots,b \tag{6}$$

the matrix form will be:

$$(\boldsymbol{q}_i)_{c\times 1} = (\mathbf{H}_i)_{c\times m}(\boldsymbol{w}_i)_{m\times 1} + \boldsymbol{\varepsilon}_{c\times 1} \tag{7}$$

To calculate the weights of the above regression, the following objective function has to be minimized:

$$\min_{\boldsymbol{w}_i} \|\boldsymbol{q}_i - \mathbf{H}_i\boldsymbol{w}\|^2 + \delta\|\boldsymbol{w}_i\|^2 \;; i = 1,2,\dots,b \tag{8}$$

where δ is the regularization parameter empirically tuned. The ordinary least square is used to solve the above optimization problem. The solution will be:

$$\widehat{\boldsymbol{w}}_i = \left(\mathbf{H}_i{}^T\mathbf{H}_i + \delta\mathbf{I}\right)^{-1}\mathbf{H}_i{}^T\boldsymbol{q}_i \tag{9}$$

The estimated weight vector is normalized and composes ith column of the projection matrix $\mathbf{A}$. The RRPS method has some advantages:

1- It uses both polarimetric and contextual features.
2- It has a simple and closed form solution.
3- Due to using the first-order statistics, it is efficient for using with small training sets.
4- It produces a reduced dimensionality feature space with the lowest overlapping and redundant information.

2.2. Guided RRPS

The Reduced polarimetric-spatial cube obtained by RRPS is given to the support vector machine (SVM) [23] to obtain the initial classification map. Due to high speckle noise of SAR images, there are noisy points in the achieved classification map, which degrade the classification accuracy. To deal with this difficulty, the guided filter is used to smooth the obtained classification map. In a PolSAR image with N pixels and with C classes, the initial classification map corresponds to C binary probability maps $\{\boldsymbol{Prob}_1, \boldsymbol{Prob}_2, \dots, \boldsymbol{Prob}_C\}$ where $\boldsymbol{Prob}_i \in \mathcal{R}^{r\times c}$ is i th binary probability map. $\boldsymbol{Prob}_{i,j} = 1;\ i = 1, \dots, C; j = 1, \dots, N$ if pixel j belongs to class i; and otherwise, $\boldsymbol{Prob}_{i,j} = 0$. The probabilities values are optimized as follows:

$$\widehat{\boldsymbol{Prob}}_{i,j} = \sum_j W_{i,j}(\boldsymbol{G})\,\boldsymbol{Prob}_{i,j} \tag{10}$$

where i and j indicate the indices of the pixels i and j, respectively; $\boldsymbol{G}$ is the guidance image and $W_{i,j}(\boldsymbol{G})$ is the filtering weight computed by:

$$W_{i,j}(\boldsymbol{G}) = \frac{1}{|w|^2}\sum_{k\in w_i, k\in w_j}\left(1 + \frac{(G_i - \mu_k)(G_j - \mu_k)}{\sigma_k^2 + \varepsilon}\right) \tag{11}$$

where w_i denotes the local window around the pixel i; μ_k and σ_k are the mean and standard deviation of $\boldsymbol{G}$ in w_k , respectively; and $|w|$ denotes the number of pixels present in window w_k. The filter preserves the edges according to $\boldsymbol{G}$. The first principal component of the original PolSAR image, obtained by the PCA transform is chosen as $\boldsymbol{G}$ in this work.

The use of the weighted mean of the neighborhood probabilities, i.e., $\widehat{\boldsymbol{Prob}}_{i,j};\ i = 1, \dots, C; j = 1, \dots, N$ instead of the original probabilities $\left(\boldsymbol{Prob}_{i,j}\right)$ not only involves more contextual information in the classification process but also causes that the probability maps are aligned with the real class boundaries.

The used guided filter has two free parameters: the size of local window determined by $(2a + 1) \times (2a + 1)$ and the regularization parameter ε. The appropriate values of these free parameters are determined according to the done experiments. For more details, the interested readers are referred to [18]-[20]. If pixels i and j in a window are located on the same side of an edge, the sign of $(G_i - \mu_k)\left(G_j - \mu_k\right)$ will be positive. Otherwise, it is negative. So, a larger weight is assigned to each pair of pixels on the same side of an edge and wise versa. Therefore, the probabilities of pixels on the same side of an edge will be similar. After filtering of the probability maps, the label of pixel j is determined by using the maximum decision rule as follows:

$$l_j = \arg\max_{i=1,\dots,C} \boldsymbol{Prob}_{i,j}\,;\ j = 1, \dots, N \tag{12}$$

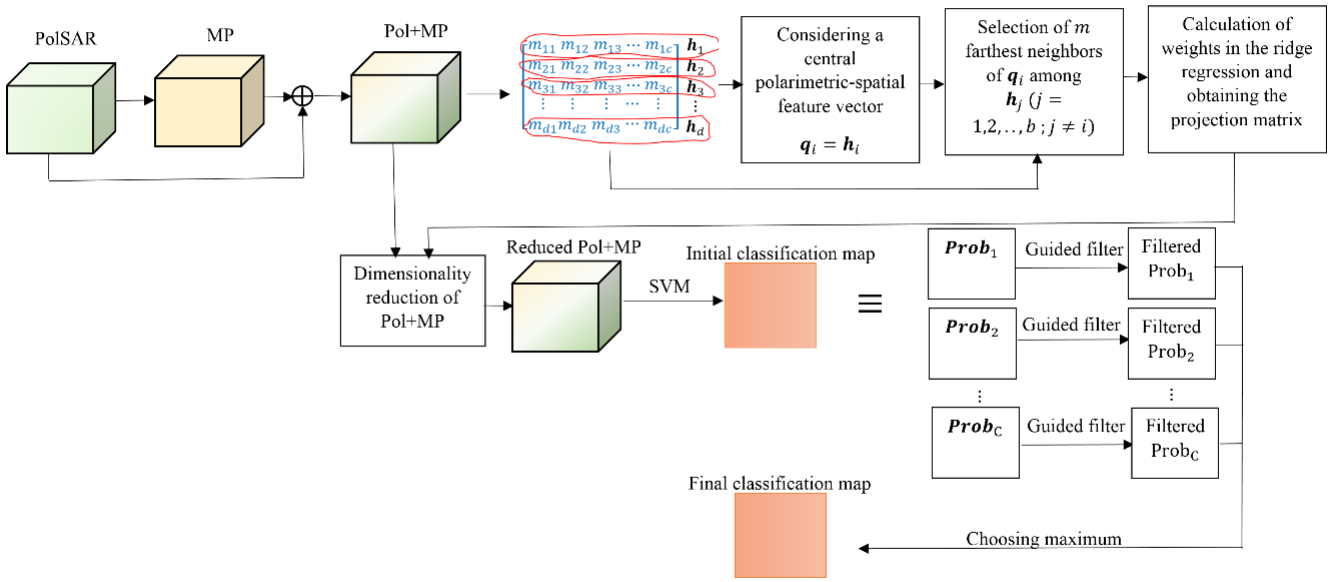

Fig. 1. Flowchart of the proposed guided RRPS method.

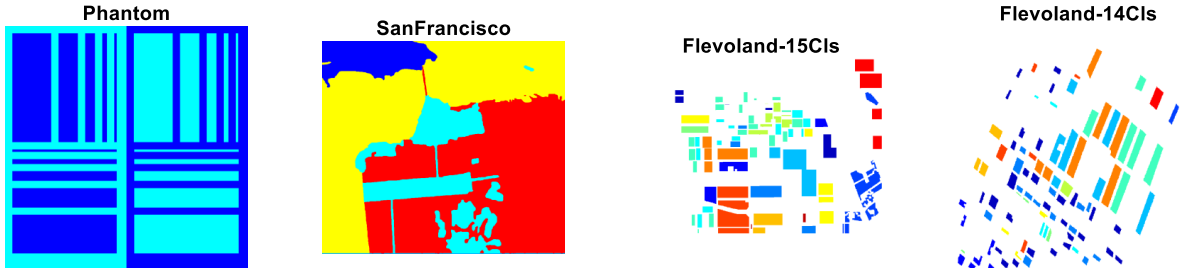

Fig. 2. Ground truth map of four datasets.

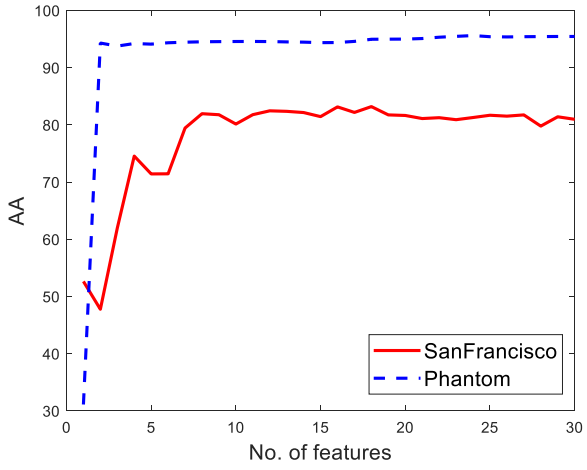

Fig. 3. Average accuracy versus the number of extracted features in the RRPS method.

Fig. 1 shows flowchart of the proposed guided RRPS method.

3. Experiments

A simulated PolSAR data and three real PolSAR images are used for doing experiments in this section. The simulated data called Phantom has two classes and 500×500 pixels [24]. The Wishart generator is used for synthesizing with the covariance matrix $\Sigma = \mu\Sigma_{k_1} + (1-\mu)\Sigma_{k_2}$ where the parameter $0 \leq \mu \leq 1$ controls how much two classes are mixed. $\mu = 0$ represents no mixture and $\mu = 1$ is equal to full mixture. $\mu = 0.7$ is used to synthesize the Phantom data in this work.

The first real dataset is the SanFrancisco Bay image acquired by L-band AIRSAR containing four classes and 900×1024 pixels [25]. The third and fourth real datasets are also acquired by L-band AIRSAR but over Flevoland in Netherlands [26], which is an agriculture area. Flevoland-15Cls contains 15 classes and 750×1024 pixels while Flevoland-14Cls contains14 classes and 1020×1024 pixels. The ground truth maps (GTM) of four datasets are shown in Fig. 2.

The proposed method is compared with Pol, MP, Pol+MP, FPs and LE-IF where Pol means the original PolSAR cube, MP is the morphological profile and Pol+MP is the concatenation of Pol and MP. The SVM classifier with the polynomial kernel of third degree is implemented for PolSAR image classification in all methods. To evaluate performance of the feature extraction methods in small sample size situations, just 5 training samples per class are used in all methods and all datasets. Training samples are randomly selected from the entire scene and the remained samples are used as testing data. The experiments are repeated 20 times and the average results are reported.

Table 1. Classification results achieved by using 5 training samples per class for Phantom dataset.

No	Name of class	# Total Samples	RPSP	Guided RPSP	Pol	MP	Pol+MP	FPs	LE-IF
1	Dark blue	125000	99.55	99.84	100.00	100.00	99.51	99.16	100.00
2	Light blue	125000	88.95	93.11	84.92	78.95	87.61	88.23	76.87
Average Accuracy			94.25	96.48	92.46	89.47	93.56	93.70	88.44
Overall Accuracy			94.25	96.48	92.46	89.47	93.56	93.70	88.44
Kappa Coefficient			88.50	92.96	84.92	78.94	87.12	87.39	76.87

Table 2. McNemars test results achieved by using 5 training samples per class for Phantom dataset.

	RRPS	Guided RRPS	Pol	MP	Pol+MP	FPs	LE-IF
RRPS	0	-67.79	44.55	104.54	27.05	20.09	111.55
Guided RRPS	67.79	0	93.33	130.91	81.48	78.39	137.20
Pol	-44.55	-93.33	0	80.80	-28.09	-30.01	87.37
MP	-104.54	-130.91	-80.80	0	-95.03	-93.51	30.70
Pol+MP	-27.05	-81.48	28.09	95.03	0	-9.04	96.23
FPs	-20.09	-78.39	30.01	93.51	9.04	0	95.63
LE-IF	-111.55	-137.20	-87.37	-30.70	-96.23	-95.63	0

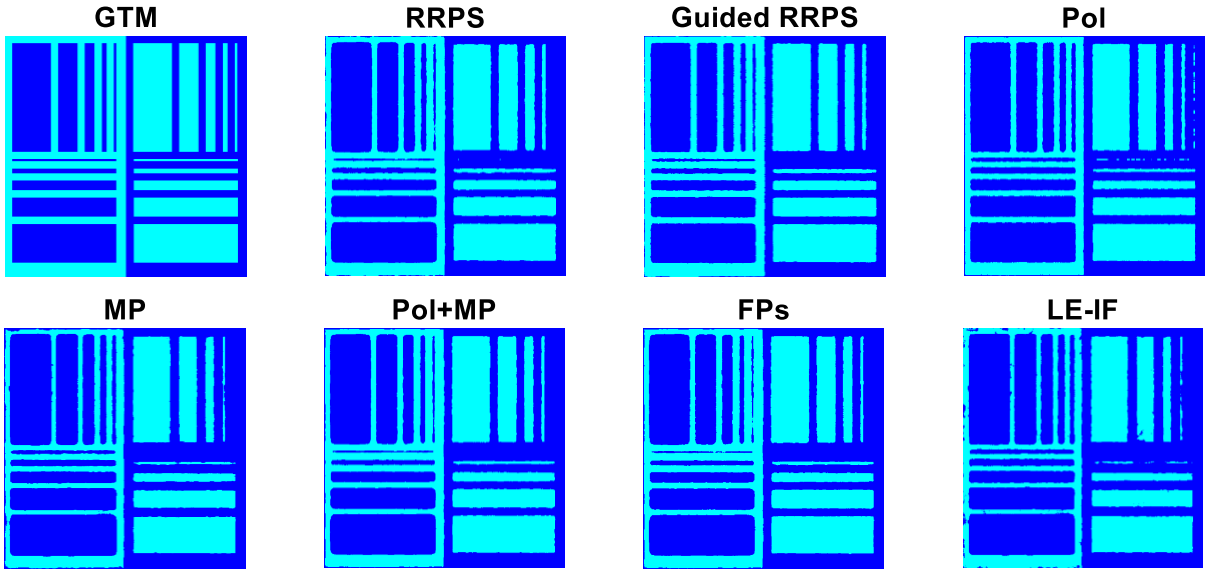

Fig. 4. GTM and classification maps obtained for Phantom dataset.

Table 3. Classification results achieved by using 5 training samples per class for the SanFrancisco dataset.

No	Name of class	# Total Samples	RPSP	Guided RPSP	Pol	MP	Pol+MP	FPs	LE-IF
1	Mountain	61913	87.97	92.16	66.64	78.11	85.45	85.79	91.47
2	Grass	135282	75.25	78.37	48.21	63.21	70.00	68.09	62.63
3	Sea	348639	86.43	91.49	83.25	80.95	82.52	82.70	80.43
4	Building	375766	73.83	84.95	81.44	75.08	78.35	76.67	78.80
Average Accuracy			80.87	86.74	69.89	74.34	79.08	78.31	78.33
Overall Accuracy			79.76	86.94	76.25	75.76	79.18	78.30	77.90
Kappa Coefficient			71.15	80.77	65.59	65.59	70.03	68.87	68.30

Table 4. McNemars test results achieved by using 5 training samples per class for the SanFrancisco dataset.

	RRPS	Guided RRPS	Pol	MP	Pol+MP	FPs	LE-IF
RRPS	0	-181.82	75.06	89.43	13.92	34.18	41.93
Guided RRPS	181.82	0	231.84	240.29	180.67	196.96	201.86
Pol	-75.06	-231.84	0	10.24	-62.47	-42.77	-34.92
MP	-89.43	-240.29	-10.24	0	-132.27	-91.93	-62.44
Pol+MP	-13.92	-180.67	62.47	132.27	0	43.22	39.44
FPs	-34.18	-196.96	42.77	91.93	-43.22	0	11.84
LE-IF	-41.93	-201.86	34.92	62.44	-39.44	-11.84	0

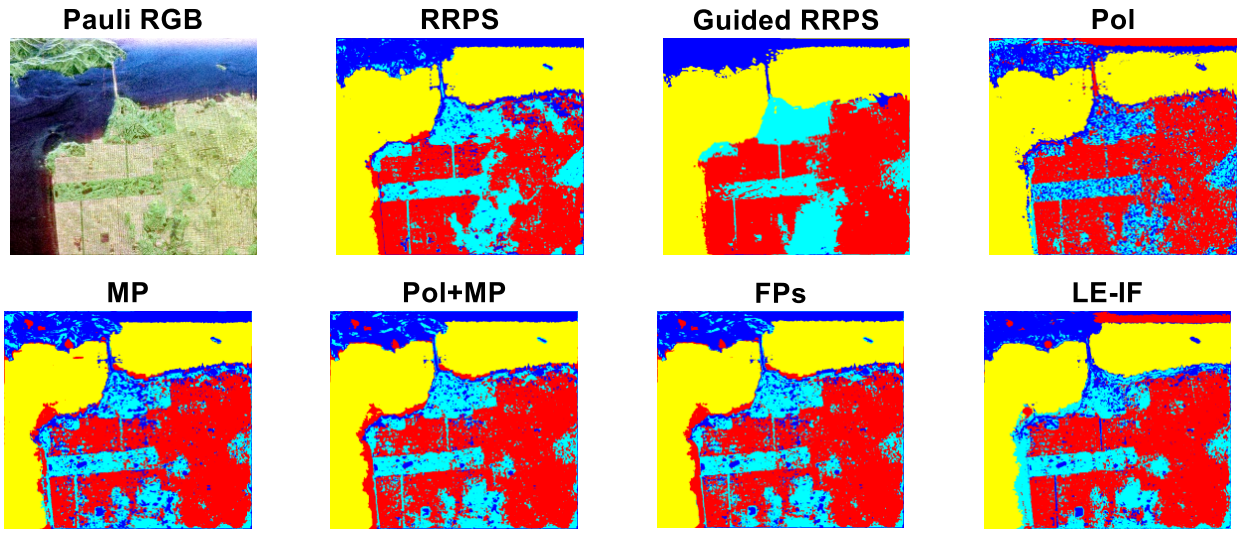

Fig. 5. Pauli RGB and classification maps obtained for SanFrancisco dataset.

Table 5. Classification results achieved by using 5 training samples per class for Flevoland-15Cls dataset.

No	Name of class	# Total Samples	RPSP	Guided RPSP	Pol	MP	Pol+MP	FPs	LE-IF
1	Stembeans	6103	92.59	95.40	89.92	92.43	94.18	92.66	92.91
2	Peas	9111	96.39	99.86	95.91	98.44	98.42	98.44	98.25
3	Forest	14944	96.14	99.93	61.60	94.04	94.31	95.38	92.77
4	Lucerne	9477	76.65	75.57	62.25	75.26	77.79	80.61	72.61
5	Wheat	17283	95.15	99.87	74.92	83.55	93.30	98.98	91.75
6	Beet	10050	84.67	82.80	55.48	34.01	42.42	39.42	32.72
7	Potatoes	15292	93.16	99.44	50.42	92.11	91.92	92.15	93.81
8	Bare soil	3078	99.97	100.00	97.89	100.00	100.00	100.00	100.00
9	Grass	6269	47.09	59.77	45.54	47.50	49.48	68.02	45.56
10	Rapeseed	12690	80.47	86.38	67.68	46.32	40.74	39.28	39.24
11	Barely	7156	94.93	99.15	86.08	95.26	95.43	95.43	95.54
12	Wheat 2	10591	85.56	97.21	85.70	86.28	93.59	96.73	89.97
13	Wheat 3	21300	63.03	61.00	69.77	68.47	70.96	70.96	71.21
14	Water	13476	82.98	82.81	66.90	66.25	66.38	67.23	66.19
15	Buildings	476	82.14	86.97	79.41	82.35	82.56	83.19	81.30
Average Accuracy			84.73	88.41	72.63	77.49	79.43	81.23	77.59
Overall Accuracy			84.15	87.44	69.62	75.99	78.30	79.88	76.68
Kappa Coefficient			82.75	86.34	66.93	73.91	76.41	78.12	74.60

Table 6. McNemars test results achieved by using 5 training samples per class for Flevoland-15Cls dataset.

	RRPS	Guided RRPS	Pol	MP	Pol+MP	FPs	LE-IF
RRPS	0	-50.14	112.77	85.16	63.78	46.10	78.69
Guided RRPS	50.14	0	136.68	117.45	98.59	82.99	110.12
Pol	-112.77	-136.68	0	-46.64	-65.25	-76.99	-52.09
MP	-85.16	-117.45	46.64	0	-41.29	-60.02	-11.37
Pol+MP	-63.78	-98.59	65.25	41.29	0	-34.94	31.41
FPs	-46.10	-82.99	76.99	60.02	34.94	0	54.56
LE-IF	-78.69	-110.12	52.09	11.37	-31.41	-54.56	0

3.1. Parameter settings

With using low number of PCs, low polarimetric information of the PolSAR data is included in the classification process while with using the high number of PCs, not only the computational burden of the proposed method is increased but also some redundant information may be generated in the spatial feature extraction process. In this work, Three PCs of the PolSAR cube are used for providing the MP in these methods: MP, Pol+MP, RRPS and guided RRPS. For generating the MP, there is a similar explanation. Applying low number of morphological filters does not provide sufficient spatial features while applying high number of morphological operators leads to high computational burden and providing redundant spatial information. 32 opening filters by reconstruction, 32 closing filters by reconstruction and the associated PC compose a MP with 65 channels from each PC of the PolSAR cube.

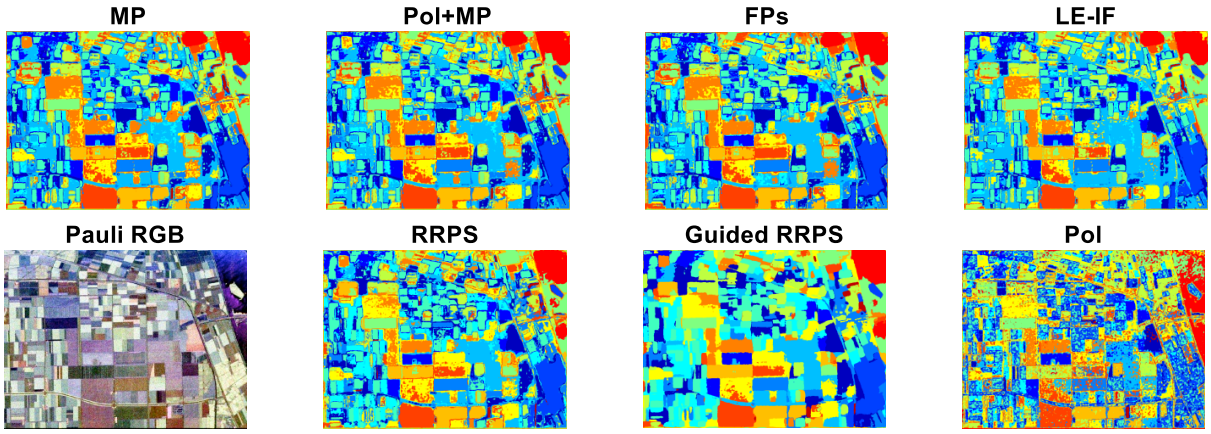

Fig. 6. Pauli RGB and classification maps obtained for Flevoland-15Cls dataset.

Table 7. Classification results achieved by using 5 training samples per class for Flevoland-14Cls dataset.

No	Name of class	# Total Samples	RPSP	Guided RPSP	Pol	MP	Pol+MP	FPs	LE-IF
1	Potato	21613	95.98	98.68	92.52	50.11	77.17	74.06	82.22
2	Fruit	4352	94.99	96.83	95.01	95.98	96.12	96.16	95.82
3	Oats	1394	93.26	100.00	80.77	95.41	98.78	99.64	98.78
4	Beet	10817	51.14	50.05	50.70	40.39	40.08	39.97	28.27
5	Barley	24543	66.09	72.40	51.40	16.04	57.56	56.98	53.17
6	Onions	2130	43.90	37.28	46.76	0.28	46.76	46.76	49.39
7	Wheat	26277	89.20	97.93	93.03	47.04	97.97	97.34	83.36
8	Beans	1082	90.76	62.01	67.65	11.65	98.15	98.34	91.68
9	Peas	2160	99.49	99.03	100.00	99.95	98.75	97.73	98.01
10	Maize	1290	96.20	90.93	85.35	97.75	98.53	98.76	69.22
11	Flax	4301	96.61	99.67	98.16	93.89	96.00	96.02	96.09
12	Rapeseed	28235	93.26	98.41	93.87	55.58	96.51	96.43	95.92
13	Grass	4204	83.40	93.39	84.23	17.58	83.18	83.87	61.49
14	Lucerne	2952	89.02	99.42	83.33	82.05	85.20	85.30	81.40
Average Accuracy			84.52	85.43	80.20	57.41	83.63	83.38	77.49
Overall Accuracy			83.71	88.34	80.91	46.88	80.75	80.03	75.80
Kappa Coefficient			81.11	86.40	77.79	41.08	77.80	76.99	72.27

Table 8. McNemars test results achieved by using 5 training samples per class for Flevoland-14Cls dataset.

	RRPS	Guided RRPS	Pol	MP	Pol+MP	FPs	LE-IF
RRPS	0	-57.71	25.86	211.37	29.43	36.22	69.69
Guided RRPS	57.71	0	71.29	229.74	74.09	80.04	107.21
Pol	-25.86	-71.29	0	200.28	1.45	7.92	42.78
MP	-211.37	-229.74	-200.28	0	-206.44	-204.87	-183.84
Pol+MP	-29.43	-74.09	-1.45	206.44	0	17.64	59.23
FPs	-36.22	-80.04	-7.92	204.87	-17.64	0	49.84
LE-IF	-69.69	-107.21	-42.78	183.84	-59.23	-49.84	0

According to done experiments, the regularization parameter is set as $\delta = 10^{-4}$ in the proposed RRPS and guided RRPS methods. The average accuracy (AA) versus the number of extracted features (m) obtained for the RRPS method is shown in Fig. 3 for Phantom and SanFrancisco datasets. As expected, with increasing the number of extracted features, more polarimetric-spatial features are involved in the classification process, and so, AA is increased. But, from a point to next, with increasing m, redundant information contained in overlapped features is included in the feature space, which degrades the classification accuracy.

The parameters of the guided filter in the guided RRPS method are also selected as follows: $\varepsilon = 10^{-5}$ in all datasets; $a = 65$ in the SanFrancisco dataset and $a = 18$ in other datasets. More explanations about the effects of the free parameters of the guided filter can be found in [18]-[20].

3.2. Classification Results

The RRPS and the guided RRPS methods are compared with the Pol, MP, Pol+MP, FPs and LE-IF methods. The comparison between the methods is done in terms of classification accuracy per class, average accuracy, overall

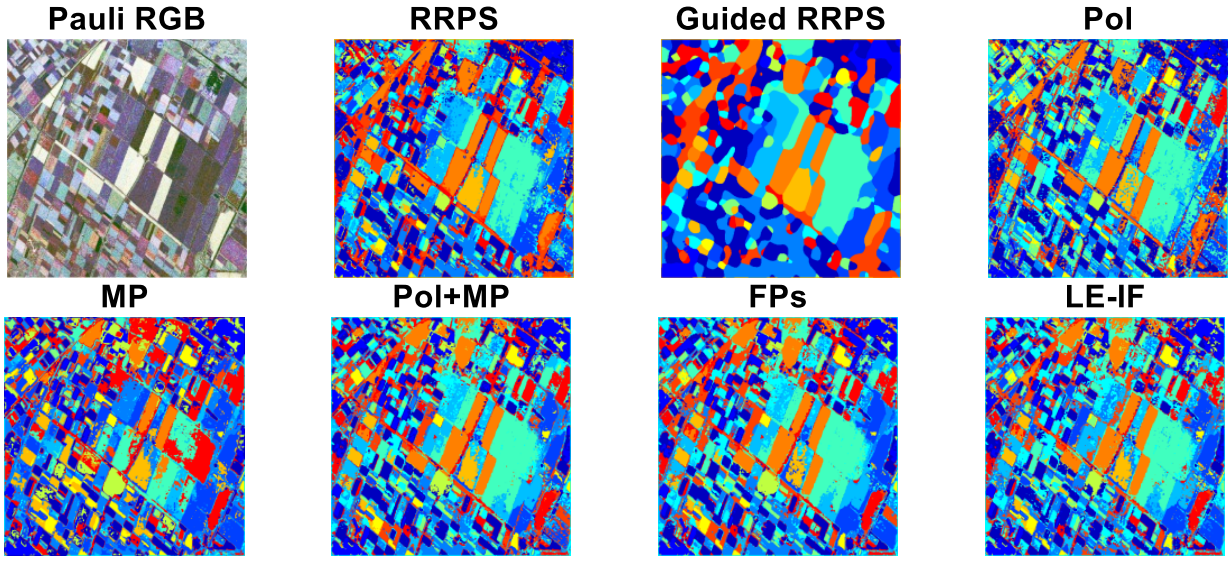

Fig. 7. Pauli RGB and classification maps obtained for Flevoland-14Cls dataset.

accuracy and kappa coefficient. The kappa coefficient is computed by [27]:

$$Kappa = \frac{N\sum_{i=1}^{C} t_{ii} - \sum_{i=1}^{C} t_{i+}t_{+i}}{N^2 - \sum_{i=1}^{C} t_{i+}t_{+i}} \quad (13)$$

where N and C indicate the number of testing samples and the number of classes respectively. t_{ii} denotes the number of pixels correctly classified in class i; t_{i+} is the number of testing pixels labeled as class i while t_{+i} is the number of pixels predicted as class i. In addition, the McNemars test is done to show whether differences between each pair of methods are statistically significant or not. The parameter Z_{12} defined in McNemars test is based upon the standardized normal test statistic calculated by [28]:

$$Z_{12} = \frac{f_{12} - f_{21}}{\sqrt{f_{12} + f_{21}}} \quad (14)$$

where f_{12} is the number of pixels correctly classified by method 1 and incorrectly by method 2. The difference between the classification accuracy of two classifiers is statistically significant if $|Z_{12}| > 1.96$ where the sign of parameter Z_{12} represents whether the classifier 1 outperforms the classifier 2 ($Z_{12} > 0$) or not ($Z_{12} < 0$).

The classification and McNemars test results for the Phantom dataset are reported in Tables 1-2. The guided RRPS is the best method with a significant difference with respect to other methods. RRPS ranks second. FPs and Pol+MP are other preferred methods. The original Pol cube provides higher classification accuracy compared to MP. The classification maps are shown in Fig. 4. The achieved results for the SanFrancisco image are reported in Tables 3-4. The best methods rank as follows: guided RRPS, RRPS, Pol+MP and FPs. GTM, Pauli RGB and the classification maps are shown in Fig. 5. The classification and McNemars test results for the Flevolans-15Cls datasets are represented in Tables 5-6. According to the obtained results, the difference among the guided RRPS and RRPS methods and the competitors are actually great. In this dataset, the MP works much better than Pol. This may be due to high noise present in Flevoland-15Cls PolSAR image. Fig. 6 shows the classification maps. The achieved results for Flevolan-14CLs are reported in Tables 7-8 and Fig. 7. In this dataset, MP fails to work properly. It means that the significance of polarimetric information in this dataset is high. As seen, after guided RRPS and RRPS, Pol provides the best classification results.

4. Conclusion

The proposed RRPS method and its revised version, guided RRPS, result in a reduced dimensionality polarimetric-morphological feature space. Due to selection of the farthest neighbors of each polarimetric-morphological channel, the generated features contain the lowest redundant information. Each channel is represented by a mean vector of training samples in that channel and there is no requirement to calculate the second-order statistics. So, RRPS and guided RRPS have a superior performance by using a small training set. Moreover, RRPS has a closed-form solution with simple implementation. The experiments are done on one synthetic dataset and three real PolSAR images.

According to the experimental results, generally, the proposed guided RRPRS and RRPS methods achieve the highest classification accuracy in terms of average accuracy, overall accuracy, and kappa coefficient. As seen, according to the McNemars test, they are preferred with respect to others with a significant difference from the statistical point of view. After guided RRPS and RRPS methods, FPs and Pol+MP can be good candidates for PolSAR image classification in all datasets. Although FPs can provide good classification accuracy from the quantity measures point of view, its classification map is noisier than the classification map of RRPS. More appropriate fusion of polarimetric and

morphological features instead of the simple stacking approach can be studied in future works for generating the initial polarimetric-spatial cube. In addition, instead of the morphological filters, more appropriate spatial filters can be studied for contextual feature extraction from the PolSAR images.

References

[1] A. Liu, F. Wang, H. Xu and L. Li, "N-SAR: A New Multichannel Multimode Polarimetric Airborne SAR," in *IEEE Journal of Selected Topics in Applied Earth Observations and Remote Sensing*, vol. 11, no. 9, pp. 3155-3166, Sept. 2018.

[2] M. Ahishali, S. Kiranyaz, T. Ince and M. Gabbouj, "Multifrequency Polsar Image Classification Using Dual-Band 1D Convolutional Neural Networks," *2020 Mediterranean and Middle-East Geoscience and Remote Sensing Symposium (M2GARSS)*, Tunis, Tunisia, pp. 73-76, 2020.

[3] P. A. A. Penna and N. D. A. Mascarenhas, "SAR Speckle Nonlocal Filtering With Statistical Modeling of Haar Wavelet Coefficients and Stochastic Distances," in *IEEE Transactions on Geoscience and Remote Sensing*, vol. 57, no. 9, pp. 7194-7208, Sept. 2019.

[4] S. Wang, J. Pei, K. Liu, S. Zhang and B. Chen, "Unsupervised classification of POLSAR data based on the polarimetric decomposition and the co-polarization ratio," *2011 IEEE International Geoscience and Remote Sensing Symposium*, Vancouver, BC, pp. 424-427, 2011.

[5] H. Maurya and R. K. Panigrahi, "PolSAR image classification using generalized scattering models," *2017 Progress in Electromagnetics Research Symposium - Fall (PIERS - FALL)*, Singapore, pp. 408-412, 2017.

[6] S. T. Tu, J. Y. Chen, W. Yang and H. Sun, "Laplacian Eigenmaps-Based Polarimetric Dimensionality Reduction for SAR Image Classification," in *IEEE Transactions on Geoscience and Remote Sensing*, vol. 50, no. 1, pp. 170-179, Jan. 2012.

[7] L. Zhang, L. Sun and W. M. Moon, "Polarimetric SAR image classification based on contextual sparse representation," *2015 IEEE International Geoscience and Remote Sensing Symposium (IGARSS)*, Milan, pp. 1837-1840, 2015.

[8] H. Bi, L. Xu, X. Cao, Y. Xue and Z. Xu, "Polarimetric SAR Image Semantic Segmentation With 3D Discrete Wavelet Transform and Markov Random Field," in *IEEE Transactions on Image Processing*, vol. 29, pp. 6601-6614, 2020.

[9] A. Masjedi, M. J. Valadan Zoej and Y. Maghsoudi, "Classification of Polarimetric SAR Images Based on Modeling Contextual Information and Using Texture Features," in *IEEE Transactions on Geoscience and Remote Sensing*, vol. 54, no. 2, pp. 932-943, Feb. 2016.

[10] B. Zou, X. Xu and L. Zhang, "Object-Based Classification of PolSAR Images Based on Spatial and Semantic Features," in *IEEE Journal of Selected Topics in Applied Earth Observations and Remote Sensing*, vol. 13, pp. 609-619, 2020.

[11] A. Tombak, İ. Türkmenli, E. Aptoula and K. Kayabol, "Pixel-Based Classification of SAR Images Using Feature Attribute Profiles," in *IEEE Geoscience and Remote Sensing Letters*, vol. 16, no. 4, pp. 564-567, April 2019.

[12] P. Zhang, B. Li, X. Tan, Y. Jiang, M. Li and Y. Wu, "Hybrid Conditional Random Fields Based on Complex-valued 3D CNN for PolSAR Image Classification," *2020 IEEE Radar Conference (RadarConf20)*, 2020, pp. 1-6.

[13] X. Nie, R. Gao, R. Wang and D. Xiang, "Online Multiview Deep Forest for Remote Sensing Image Classification via Data Fusion," in *IEEE Geoscience and Remote Sensing Letters*, vol. 18, no. 8, pp. 1456-1460, Aug. 2021.

[14] X. Mao, X. Xiao and Y. Lu, "PolSAR Data-Based Land Cover Classification Using Dual-Channel Watershed Region-Merging Segmentation and Bagging-ELM," in *IEEE Geoscience and Remote Sensing Letters*, In Press, 2021.

[15] R. Sharma and R. K. Panigrahi, "Texture Classification-Based NLM PolSAR Filter," in *IEEE Geoscience and Remote Sensing Letters*, vol. 18, no. 8, pp. 1396-1400, Aug. 2021.

[16] M. Imani and H. Ghassemian, "Morphology-based structure-preserving projection for spectral–spatial feature extraction and classification of hyperspectral data," IET Image Processing, vol. 13, no. 2, pp. 270-279, Feb. 2019.

[17] K. Cho, S. Park, J. Cho, H. Moon and S. Han, "Automatic Urban Area Extraction From SAR Image Based on Morphological Operator," in *IEEE Geoscience and Remote Sensing Letters*, 2020.

[18] X. Kang, S. Li and J. A. Benediktsson, "Spectral–Spatial Hyperspectral Image Classification With Edge-Preserving Filtering," in *IEEE Transactions on Geoscience and Remote Sensing*, vol. 52, no. 5, pp. 2666-2677, May 2014.

[19] X. Kang, S. Li and J. A. Benediktsson, "Feature Extraction of Hyperspectral Images With Image Fusion and Recursive Filtering," in *IEEE Transactions on Geoscience and Remote Sensing*, vol. 52, no. 6, pp. 3742-3752, June 2014.

[20] M. Imani, "A Random Patches Based Edge Preserving Network for Land Cover Classification Using Polarimetric Synthetic Aperture Radar Images," International Journal of Remote Sensing, 2021.

[21] M. Imani and H. Ghassemian, "Ridge regression-based feature extraction for hyperspectral data," International Journal of Remote Sensing, vol. 36, no. 6, pp. 1728–1742, 2015.

[22] Qingfu Zhang and Yiu Wing Leung, "A class of learning algorithms for principal component analysis and minor component analysis," in *IEEE Transactions on Neural Networks*, vol. 11, no. 1, pp. 200-204, Jan. 2000.

[23] M. Imani and H. Ghassemian, "The Investigation of Sensitivity of SVM Classifier Respect to The Number of Features and The Number of Training Samples," 2nd International Conference on Sensors and Models in Photogrammetry and Remote Sensing, Tehran, Iran, pp. 209-214, 5 – 8 October 2013.

[24] L. Gomez, L. Alvarez, L. Mazorra and A. C. Frery, "Fully PolSAR image classification using machine learning techniques and reaction-diffusion systems," Neurocomputing, vol. 255, pp. 52-60, 2017.

[25] X. Nie, S. Ding, X. Huang, H. Qiao, B. Zhang and Z. -P. Jiang, "An Online Multiview Learning Algorithm for PolSAR Data Real-Time Classification," in *IEEE Journal of Selected Topics in Applied Earth Observations and Remote Sensing*, vol. 12, no. 1, pp. 302-320, Jan. 2019.

[26] Z. Zhang, H. Wang, F. Xu and Y. Jin, "Complex-Valued Convolutional Neural Network and Its Application in Polarimetric SAR Image Classification," in *IEEE Transactions on Geoscience and Remote Sensing*, vol. 55, no. 12, pp. 7177-7188, Dec. 2017.

[27] J. Cohen, "A coefficient of agreement from nominal scales," *Edu. Psychol. Meas.*, vol. 20, no. 1, pp. 37–46, 1960.
[28] G. M. Foody, "Thematic map comparison: Evaluating the statistical significance of differences in classification accuracy," *Photogramm. Eng. Remote Sens.*, vol. 70, no. 5, pp. 627–633, 2004.

Maryam Imani received the B.Sc. and M.Sc. degrees in electrical engineering from Shahed University, Tehran, Iran, and the Ph.D. degree in electrical engineering from Tarbiat Modares University, Tehran, Iran in 2009, 2011, and 2015 respectively. She continued her research in Tarbiat Modares University as a postdoc. Since 2018, she has been with Tarbiat Modares University in Tehran, Iran, where she is an Assistant Professor of Electrical and Computer Engineering. Her research interests include pattern recognition, signal and image processing, and remote sensing.
Email: maryam.imani@modares.ac.ir

Paper Handling Data:

Submitted: 04-20-2021
Received in revised form: 10-19-2021
Accepted: 11-06-2021
Corresponding author: Maryam Imani
Affiliation of the corresponding author: Tarbiat Modares University